Electronic Supplementary Material (ESI) for Nanoscale.

Supporting Information

Understanding Charge Transport in Wavy Two-Dimensional Covalent Organic Frameworks

Marta Martínez-Abadía,[a] Karol Strutyński,[b] Craig T. Stoppiello,[c,d] Belén Lerma Berlanga,[e] Carlos Martí-Gastaldo,[e] Andrei N. Khlobystov,[c,d] Akinori Saeki,[f] Manuel Melle-Franco,[b] and Aurelio Mateo-Alonso*[a,g]

[a] *POLYMAT, University of the Basque Country UPV/EHU, Avenida de Tolosa 72, E-20018 Donostia-San Sebastian, Spain.*

[b] *CICECO - Aveiro Institute of Materials, Department of Chemistry, University of Aveiro, 3810-193 Aveiro, Portugal.*

[c] *School of Chemistry, University of Nottingham, University Park, Nottingham NG7 2RD, UK.*

[d] *The Nanoscale and Microscale Research Centre, University of Nottingham, University Park, Nottingham NG7 2RD, UK.*

[e] *Instituto de Ciencia Molecular, Universidad de Valencia, 46980 Paterna, Spain.*

[f] *Department of Applied Chemistry, Graduate School of Engineering, Osaka University, Suita, Osaka 565-0871, Japan.*

[g] *Ikerbasque, Basque Foundation for Science, Bilbao, Spain.*

Email: amateo@polymat.eu;

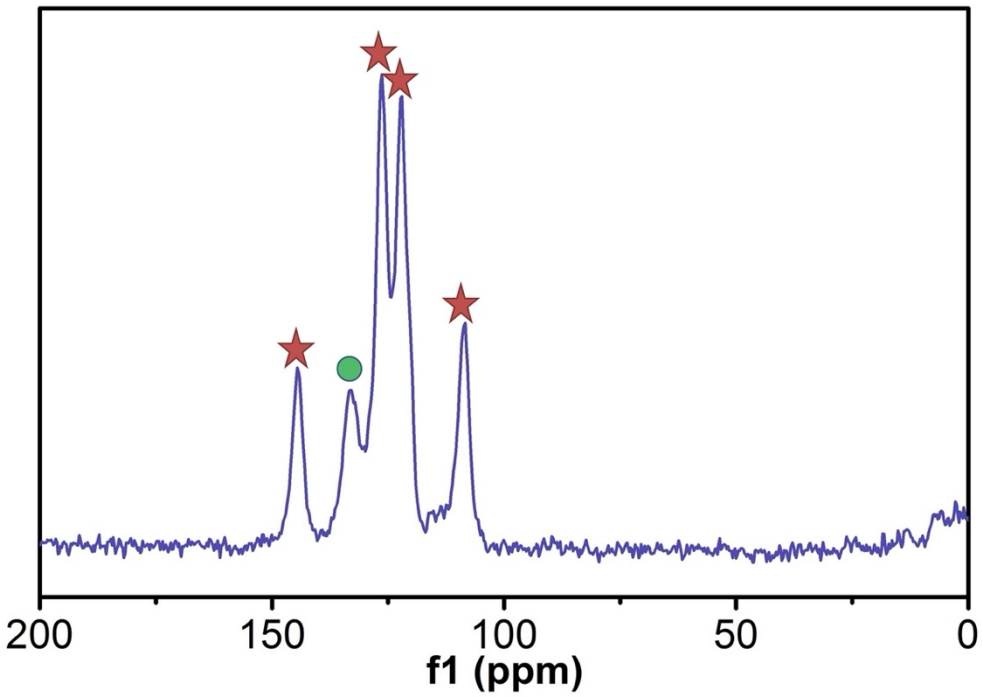

Figure S1. SS ^{13}C NMR Spectrum of Marta-COF-2. Where the stars indicate the peaks that correspond to the HBC nodes and the circles indicate the peaks that correspond to the benzene linkers.

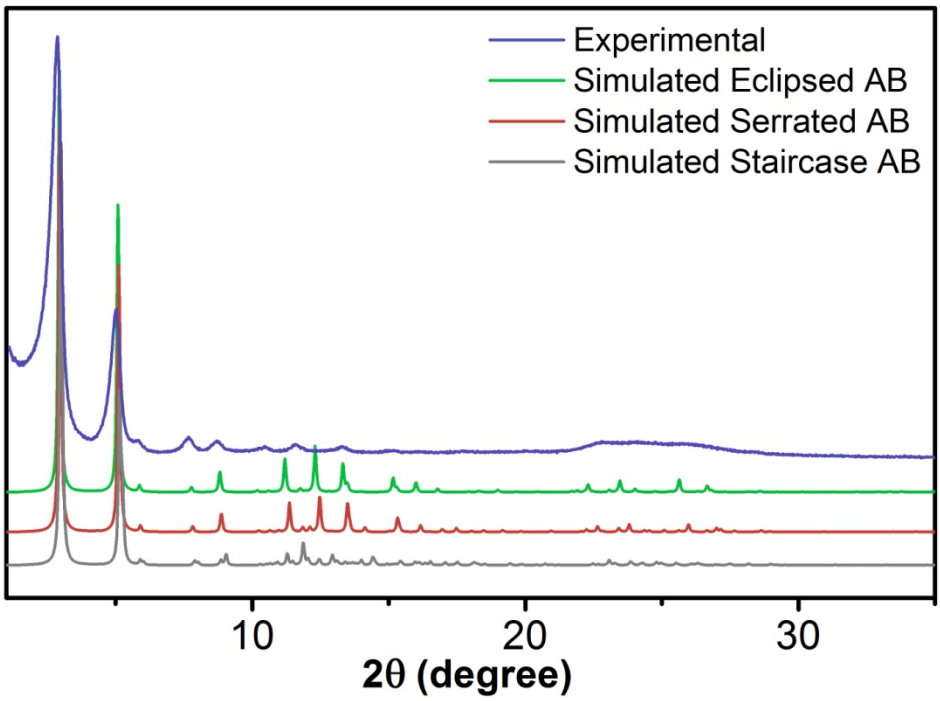

Figure S2. Experimental PXRD pattern (blue line), simulated diffraction PXRD pattern for the simulated perfectly eclipsed AB (green line), serrated AB (red line) and staircase AB (grey line) stacking of Marta-COF-2.

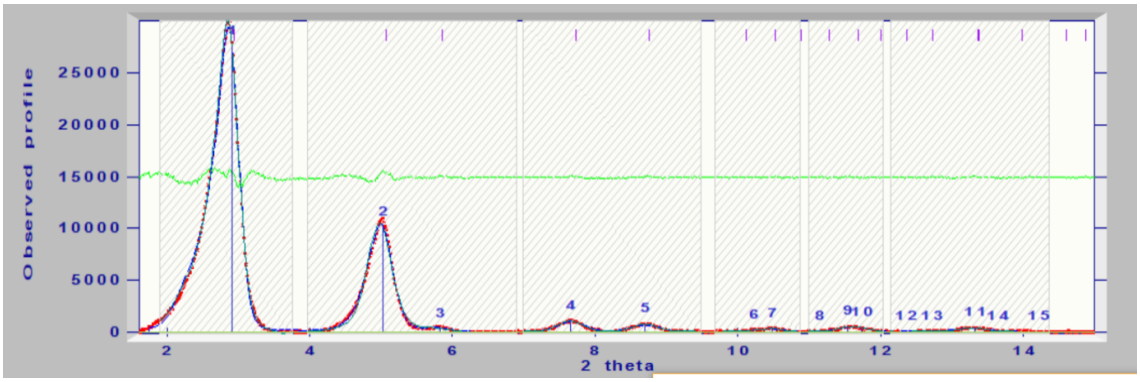

Figure S3. PXRD analysis for Marta-COF-2 including the experimental diffraction pattern (red dashed line), Pawley refined pattern (blue line), and the difference between the refined and experimental pattern (green line).

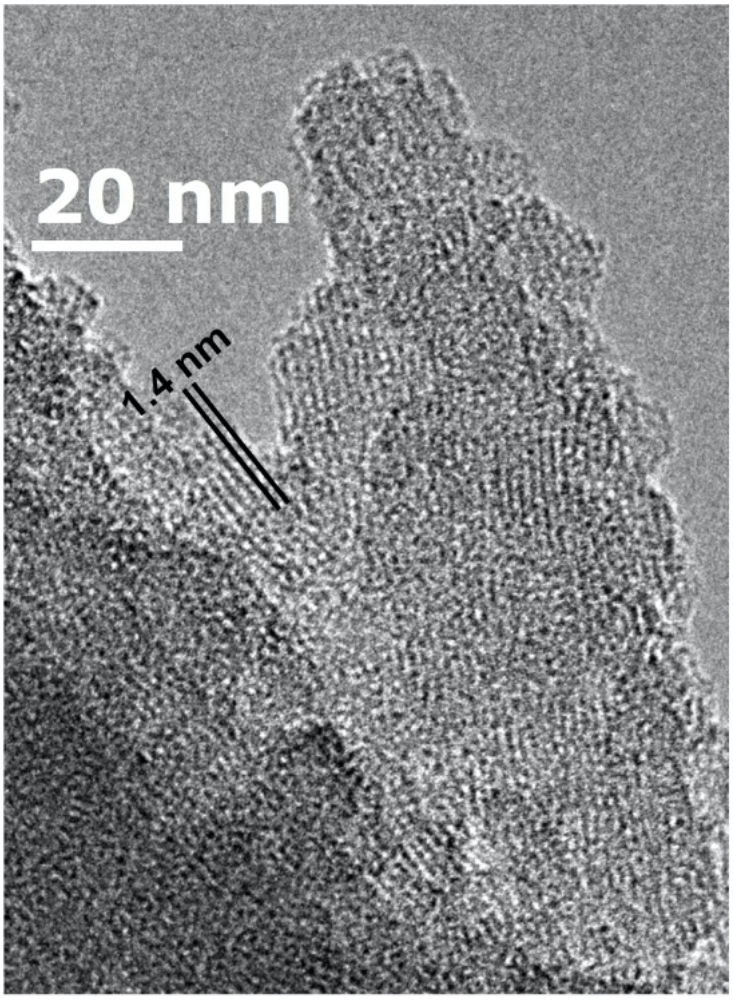

Figure S4. HR-TEM image of Marta-COF-2.

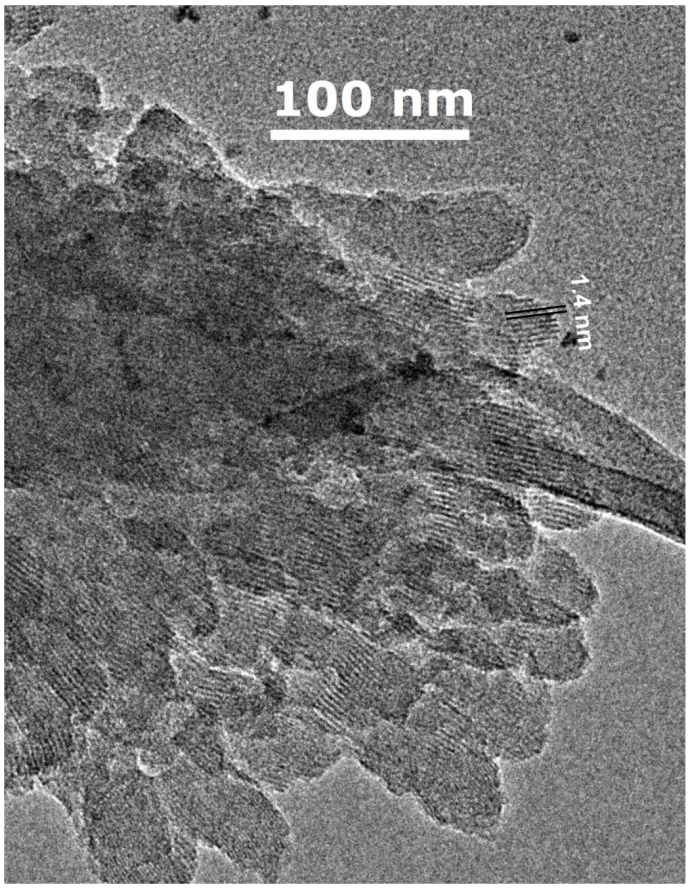

Figure S5. HR-TEM image of Marta-COF-2.

Table S1. Binding energies (BE) and gap of Marta-COF-2 obtained from DFT calculations.

System	Average ab	c	E	B3LYP Gap	BE
	Å	Å	eV	eV	kcal/mol
Monolayer	34.41	100.00	-147526.31	3.17	
AA full eclipsed	34.45	8.49	-295062.20	2.83	-218
AA serrated	34.40	8.18	-295062.79	2.61	-232
AA staircase	34.77	8.09	-295062.81	2.72	-232
AB full eclipsed	34.67	8.18	-295057.97	2.75	-121
AB serrated	34.45	8.06	-295058.20	2.78	-126
AB staircase	34.57	7.90	-295058.37	2.76	-130

Table S2. Porosity data for Marta-COF-2. The porosity, surface area and internal volume of predicted structures was calculated using PoreBlazer v4.0, with 1000 samples per atom and 0.2 Å spatial resolution.

Conformation	Density	Pore size	Surface Area	Surface Area	Probe-occupiable Volume
	g/cm^3	Å	m^2/g	m^2/cm^3	cm^3/g
AA full eclipsed	0.635	23.690	1455	924	0.929
AA serrated	0.661	22.900	1394	921	0.877
AA staircase	0.648	23.180	1400	908	0.910
AB full eclipsed	0.650	6.980	2625	1707	0.950
AB serrated	0.669	7.670	2334	1560	0.899
AB staircase	0.698	8.580	1959	1368	0.801

Experimental procedures

Reagents for synthesis were, if not otherwise specified, purchased from Aldrich, TCI or Acros Organics. Column chromatography was carried out using Silica gel 60 (40-60 μm) from Scharlab. Analytical thin layer chromatography (TLC) was done using aluminum sheets (20x20 cm) pre-coated with silica gel RP-18W 60 F254 from Merck. UV-active compounds were detected with a UV-lamp from CAMAG at wavelength λ = 254 or 366 nm. HBC was synthesized according to reported methods.[1] Marta-COF-2 was synthesized in a pre-scored 5 mL ampoule from Aldrich. For its synthesis and purification anhydrous 1,4-dioxane (99.8%), anhydrous acetone (99.8%), anhydrous hexane (97%) were purchased from Acros Organics. THF was dried using an Innovative Pure Solve solvent purification system and mesitylene (97%) was obtained from Acros Organics and dried with molecular sieves.

Solid-State ^{1}H, ^{11}B and ^{13}C CP/MAS NMR spectra were recorded on a Bruker Avance III 400 MHz NMR spectrometer at a MAS rate of 12 kHz and a CP contact time of 2 ms.

ATR-FTIR spectra were recorded on a Bruker ALPHA ATR-IR spectrometer.

The powder X-ray diffraction (PXRD) patterns were collected by using a PHILIPS X'PERT PRO automatic diffractometer operating at 40 kV and 40 mA, in theta-theta configuration, secondary monochromator with Cu-Kα radiation (λ = 1.5418 Å) and a PIXcel solid state detector (active length in 2θ 3.347º). Data were collected from 1 to 50° 2θ (step size = 0.026 and time per step = 300 s, total time 40 min) at room temperature. A variable divergence slit, giving a constant 4.0 mm area of sample illumination, was used.

The pore structure was evaluated by nitrogen sorption isotherms, measured at 77 K with a Micromeritics 3Flex apparatus. The samples were degassed in an Autosorb station at and 10^{-6} Torr at 100 °C prior to analysis. Surface area, pore size and volume values were calculated from nitrogen adsorption-desorption isotherms (77 K). Specific surface area (SA) was calculated by multi-point Brunauer-Emmett-Teller (BET) method. Total pore volume was taken at P/P_0=0.96. Pore size distribution was analysed for the adsoption branch by using classical methods and a cylindrical pore model.

Electron Microscopy. All samples were prepared by dispersion in acetone and drop cast onto lacey carbon-coated copper TEM grids (Agar). High Resolution Transmission Electron Microscopy (HRTEM) analysis was performed on a JEOL2100F operating at 200 kV. The morphology of the samples was determined by taking low magnification (ca. x 30k mag) images from different regions of the specimen, and the nanoscale features were imaged using high resolution imaging (ca. x 100k mag).

FP-TRMC experiments were conducted for the sample on a quartz plate using the third harmonic generator (THG; 355 nm) of a Nd:YAG laser (Continuum Inc., Surelite II, 5–8 ns pulse duration, 10 Hz) as the excitation source (9.1×10^{15} photons cm^{-2} $pulse^{-1}$). The frequency and power of microwave were ~9.1 GHz and 3 mW, respectively. The photoconductivity transient $\Delta\sigma$ was converted to the product of the quantum yield (φ) and the sum of charge carrier mobilities $\sum\mu$ ($= \mu_+ + \mu_-$) by the formula $\varphi\sum\mu = \Delta\sigma(eI_0F_{light})^{-1}$, where e and F_{light} are the unit charge of a single electron and a correction (or filling) factor, respectively.

Synthesis and characterization

Marta-COF-2: HBC (25.42 mg, 0.0364 mmol) and benzene-1,4-diboronic acid (9.03 mg, 0.0545 mmol) were sonicated in a mixture of degassed 1,4-dioxane/mesitylene (2:1, 2.25 mL) in a pre-scored 5 mL ampoule under nitrogen. The suspension was degassed by using three freeze-pump-thaw cycles, and the ampoule was sealed off using flame and heated at 125 ºC for 3 days. Marta-COF-2 was obtained as a yellow solid (28 mg, 90 % yield), which was collected by filtration and washed five times with anhydrous tetrahydrofurane, acetone and hexane. The powder was dried at 30 ºC under vacuum for 24 hours. SS ^{1}H-NMR (δ) (ppm): 6.97. SS ^{13}C-NMR (δ) (ppm): 144.4, 133.1, 126.4, 122.1, 108.5. SS ^{11}B-NMR (δ) (ppm): 3.32 ppm. ATR-FTIR (cm^{-1}): 1522, 1462, 1348, 1334, 1234.

Modelling and predicting electronic properties

Two methods were applied to study the structure and electronic properties of Marta-COF-2: Density Functional Theory (DFT) and semi-empirical Density Functional Theory Tight Binding (TB). In order to include van der Waals interactions we used state of the art, range separated MBD@rsSCS correction on top of the PBE functional.[2,3] DFT calculations were performed with the Fritz Haber Institute *ab initio* molecular simulations (FHI-aims) package using "light" numeric atomic orbitals, which approximately correspond to TZVP level of calculations.[3-7]

Two general packing conformations, AA and AB, with three different interlayer stackings were investigated, namely: eclipsed, serrated and staircase, see Figure S6.

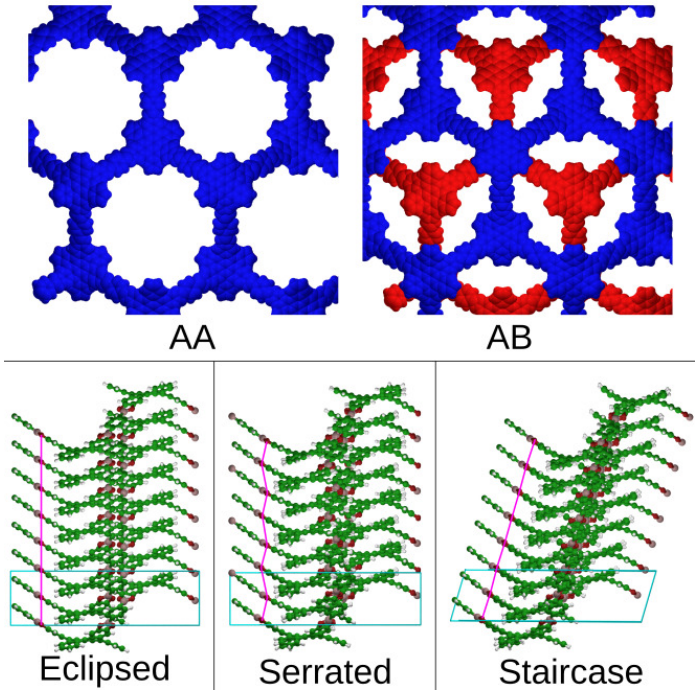

Figure S6. Conformations of Marta-COF-2. General structure (top) and possible stacking of the layers (bottom). Pink line indicates how equivalent atoms in different layers are stacked.

References

1. M. Martínez-Abadía, C. T. Stoppiello, K. Strutynski, B. Lerma-Berlanga, C. Martí-Gastaldo, A. Saeki, M. Melle-Franco, A. N. Khlobystov and A. Mateo-Alonso, A Wavy Two-Dimensional Covalent Organic Framework from Core-Twisted Polycyclic Aromatic Hydrocarbons. *J. Am. Chem. Soc.* 2019, **141**, 14403-14410.
2. Tkatchenko, A.; DiStasio, R. A.; Car, R.; Scheffler, M. Accurate and Efficient Method for Many-Body van Der Waals Interactions. *Phys. Rev. Lett.* 2012, **108**, 236402.
3. Tkatchenko, A.; Scheffler, M. Accurate Molecular Van Der Waals Interactions from Ground-State Electron Density and Free-Atom Reference Data. *Phys. Rev. Lett.* 2009, **102**, 073005.
4. Blum, V.; Gehrke, R.; Hanke, F.; Havu, P.; Havu, V.; Ren, X.; Reuter, K.; Scheffler, M. Ab Initio Molecular Simulations with Numeric Atom-Centered Orbitals. *Comput. Phys. Commun.* 2009, **180**, 2175–2196.
5. Marek, A.; Blum, V.; Johanni, R.; Havu, V.; Lang, B.; Auckenthaler, T.; Heinecke, A.; Bungartz, H.-J.; Lederer, H. The ELPA Library: Scalable Parallel Eigenvalue Solutions for Electronic Structure Theory and Computational Science. *J. Phys. Condens. Matter* 2014, **26**, 213201.
6. Yu, V. W.; Corsetti, F.; García, A.; Huhn, W. P.; Jacquelin, M.; Jia, W.; Lange, B.; Lin, L.; Lu, J.; Mi, W.; et al. ELSI: A Unified Software Interface for Kohn–Sham Electronic Structure Solvers. *Comput. Phys. Commun.* 2018, **222**, 267–285.
7. Lejaeghere, K.; Bihlmayer, G.; Björkman, T.; Blaha, P.; Blügel, S.; Blum, V.; Caliste, D.; Castelli, I. E.; Clark, S. J.; Corso, A. D.; et al. Reproducibility in Density Functional Theory Calculations of Solids. *Science* 2016, **351**, aad3000.